Rapid Self-Assembly and Sequential Infiltration Synthesis of High χ Fluorine-Containing Block Copolymers

Cian Cummins, Daniele Mantione, Federico Cruciani, Guillaume Pino, Nils Demazy, Yulin Shi, Giuseppe Portale, Georges Hadziioannou, Guillaume Fleury

Article

Rapid Self-Assembly and Sequential Infiltration Synthesis of High χ Fluorine-Containing Block Copolymers

Cian Cummins, Daniele Mantione,* Federico Cruciani, Guillaume Pino, Nils Demazy, Yulin Shi, Giuseppe Portale, Georges Hadziioannou, and Guillaume Fleury*

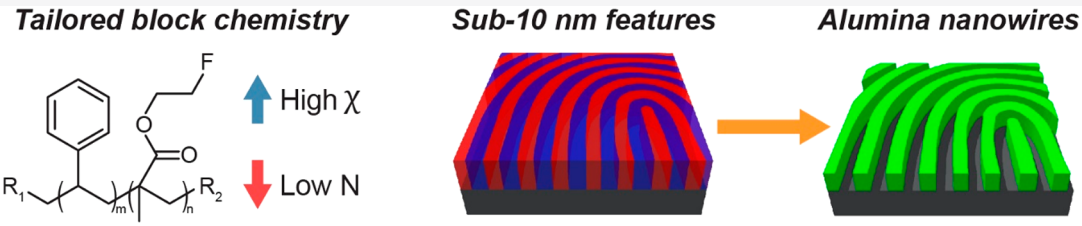

ABSTRACT: We leverage the attractive properties of a high χ–low N BCP, i.e., poly(styrene)-*block*-poly(2-fluoroethylmethyl acrylate) (PS-*b*-P2FEMA), and illustrate its utility for next-generation nanomanufacturing. The synthesis, physical characterization, and thin film self-assembly of a series of lamellar and cylindrical PS-*b*-P2FEMA BCPs are delineated. PS-*b*-P2FEMA BCPs with total molecular weights ranging from 7 to 22 kg mol^{-1} were synthesized by using reversible addition–fragmentation chain-transfer (RAFT) polymerization. Temperature-resolved small-angle X-ray scattering (SAXS) measurements revealed a large χ value (0.13 at 150 °C) for PS-*b*-P2FEMA. Solvothermal vapor annealing of PS-*b*-P2FEMA films produced highly oriented fingerprint patterns in as short as 60 s. Lamellar period sizes ranged from 25.9 down to 14.2 nm with feature sizes as small as 7 nm observed. We also demonstrate the integration feasibility of PS-*b*-P2FEMA BCPs through alumina hardmask formation using sequential infiltration synthesis. The highly favorable characteristics of the P2FEMA-based BCPs detailed here provide a versatile material option to the current library of available BCPs for sub-10 nm nanolithography.

INTRODUCTION

Thin film block copolymer (BCP) self-assembly is a powerful means to fabricate nanoscale templates with diverse applications, e.g., Li-ion batteries, solar cells, waveguides, and membrane filtration among others.[1−5] Owing to the spontaneous self-assembly of BCPs, nanoscale features can be formed depending on respective volume fraction (f_i) of the constituent polymers. Morphologies of BCPs can be tailored through f_i whereby increasing one block with respect to the other transitions from spherical, cylindrical, gyroidal, and lamellar features. Aggressive scaling of semiconductor features has pushed the limits of optical lithography patterning, and there is a pressing need to develop novel materials to further advance scaling. Both in-plane and out-of-plane cylinder orientations and out-of-plane lamellar structures can be used to fabricate logic and memory features.[6,7] Directed self-assembly (DSA) of BCPs is considered a strong candidate whereby patterns are chemically or physically guided to align with respect to the substrate.[8,9] DSA-BCP technology is envisaged to complement 193 nm immersion lithography and extreme ultraviolet lithography for semiconductor and data storage needs. DSA patterning offers a tremendously attractive methodology that is regarded as low cost and CMOS compatible given the parallels with contemporary resist development (i.e., spin, bake, strip, and etch).[10] Diffraction limits of top-down optical lithography have thus led to the exploration of new material chemistries and synthetic strategies to advance scaling. In particular, novel BCPs are required to scale to smaller periods beyond the workhorse material poly(styrene)-*block*-poly(methyl methacrylate) (PS-*b*-PMMA).

Newly synthesized block copolymers (BCPs) that possess a high Flory–Huggins interaction parameter (χ) and a low degree of polymerization (N) are now needed to define ultrasmall periods for logic applications.[11] As N needs to be low for ultrasmall periods, a high χ is therefore advantageous to satisfy that the product of χ and N is greater than 10.5 to allow microphase separation.[12] To achieve this goal, novel strategies are necessary to formulate high χ–low N BCPs that also exhibit high etch contrast or an ability to selectively infiltrate a block for pattern transfer purposes.[13] In this vein, Willson and co-workers championed the use of silicon containing BCPs to

Received: May 15, 2020
Revised: June 25, 2020

reach sub-20 nm periods beyond the well-studied PS-*b*-poly(dimethylsiloxane) (PS-*b*-PDMS) system, e.g., poly(styrene-*b*-trimethylsilylstyrene-*b*-styrene), poly(trimethylsilylstyrene-*b*-lactide),[14] poly(5-vinyl-1,3-benzodioxole-*b*-pentamethyldisilylstyrene) (PVBD-*b*-PDSS),[15] and poly(trimethylsilylstyrene-*b*-*p*-methoxystyrene) (PTMSS-*b*-PMOST).[16] Furthermore, another silicon-based BCP, poly(1,1-dimethylsilacyclobutane)-*b*-PMMA (PDMSB-*b*-PMMA), was introduced by Aissou et al. to pattern sub-10 nm period sizes in 10 min under thermal annealing.[17] Hydroxystyrene-based BCP reports have shown that extremely high χ materials can be attained due to the incompatibility of constituent polymers.[18−20] For example, Wang et al. recently detailed the RAFT synthesis of poly(pentadecafluorooctyl methacrylate)-*b*-poly(hydroxystyrene) (PPDFMA-*b*-PHS) that possessed a χ of 0.48, enabling an L_0 of 9.8 nm in lamellar thin films.[21] Other notable hydroxystyrene-based BCPs include poly(3-hydroxystyrene)-*b*-poly(dimethylsiloxane) (P3HS-*b*-PDMS),[22] poly(dihydroxystyrene)-*b*-polystyrene (PDHS-*b*-PS) with an L_0 of 5.9 nm,[23] P3HS-*b*-tBuSt, and P4HS-*b*-tBuSt demonstrating an L_0 of 8.8 nm.[24] Fluorine-based BCPs also present an appealing way to facilitate the development of high χ materials and offer the possibility of fast microphase separation due to the mobility of fluorinated blocks with low coefficients of friction.[25] Because high χ BCPs typically possess vastly different chemistries (e.g., organic vs inorganic blocks), the contrast in surface free energy (SFE) can result in large scale dewetting[26] as well as preferential wetting layer formation at the polymer/air or polymer/substrate interfaces. To overcome such problematic scenarios, a novel strategy by Hayakawa and co-workers reported the use of poly(2,2,2-trifluoroethyl methacrylate) (PTFEMA) to balance SFEs with a silicon containing moiety where L_0 = 11 nm was attained and DSA demonstrated.[27] A similar approach has been employed for PS-*b*-poly[2-hydroxy-3-(2,2,2-trifluoroethylsulfanyl)propyl methacrylate] (PS-*b*-PHFMA) producing L_0 = 9.6 nm. Jo et al. showed that the synthesis of PS-*b*-poly(2,2,2-trifluoroethyl acrylate) (PS-*b*-PTFEAs) via transesterification of PS-*b*-poly(*tert*-butyl acrylate) (PS-*b*-PtBAs) resulted in an extremely high χ and demonstrated an L_0 = 10.1 nm.[28] Likewise, Li et al. exemplified the flexibility of a series of PS-*b*-poly(pentadecafluorooctyl methacrylate) (PS-*b*-PPDFMA) BCPs that were shown to self-assemble in 1 min with cylindrical systems (L_0 = 14.3 nm) showing promise for DSA.[29]

Herein, we describe the RAFT polymerization of lamellar and cylindrical PS-*b*-P2FEMA BCPs (termed SFEMA herein) for sub-10 nm nanolithography that can be patterned in a facile manner, i.e., short times and minimal processing steps. Ordered lamellar features were developed with periods ranging from 25.9 down to 14.2 nm with feature sizes as small as 7 nm. After optimization through solvothermal vapor annealing, AlO_x patterns with feature sizes of 11 nm were developed by using sequential infiltration synthesis (SIS) of SFEMA BCPs. The series of SFEMA BCPs reported in this article provides a viable pathway to 7 nm half-pitch periods and sub-10 nm BCP feature sizes that are amenable to rapid self-assembly, i.e., ≈3 min. Our work represents significant progression of the BCP nanolithography toolbox from a materials and processing standpoint of a new fluorine-containing BCP.

EXPERIMENTAL SECTION

Materials. Styrene and trifluorostyrene were purchased from Sigma-Aldrich. 2-Fluoroethanol was purchased from ABCR. All other chemicals were supplied from Fisher Scientific. TLC were performed on aluminum precoated plates (silica gel 40−60 Å 400 mesh, F254, Aldrich) using hexane:ethyl acetate (Hex:AcOEt) as eluent. Silica gel high-purity grade, pore size 60 Å, 230−400 mesh particle size 40−63 μm was used for flash column chromatography. Solvents used for solvothermal vapor annealing were purchased from Sigma-Aldrich and were used as received. The density of P2FEMA at 25 °C was measured by pycnometer. Details are described in the Supporting Information (section 1, Materials and Methods).

Synthesis of 2FEMA. To a solution of methacrylic acid (4.35 mL; 4.65 g, 54 mmol, 1.1 equiv) in 250 mL of dry DCM, DCC (12.57 g; 61 mmol, 1.3 equiv) was added and left stirring for 30 min under argon. Afterward, 2-fluoroethanol (2.75 mL; 3 g, 47 mmol, 1 equiv) and DMAP (0.969 g; 4.7 mmol, 0.17 equiv) were added, and the reaction mixture was held at 0 °C by using an ice bath. The mixture was kept for 48 h at room temperature under an argon atmosphere. After the reaction, monitored by TLC, had reached completion, the reaction mixture was filtered to eliminate the urea salts that precipitated during the reaction. The product containing filtrate was diluted with an extra 250 mL of DCM and rinsed three times with 100 mL of water. The organic phase was dried over Na_2SO_4 and concentrated. The concentrated product was then loaded onto a silica gel column and purified by flash column chromatography by using a mixture of hexane:ethyl acetate 8:2 (R_f = 0.68) to give the product as a colorless oil (5.5 g, 89%). FT-IR ν_{max}/cm^{-1}: 3108 (=C−H), 2975, 2939 (C−H), 1710 (C=O), 1474 (C=C), and 1111 (C−F). ^{1}H NMR (400 MHz, chloroform-*d*): δ 6.15 (dd, J = 1.6, 0.9 Hz, 1H), 5.59 (p, J = 1.6 Hz, 1H), 4.70−4.64 (m, 1H), 4.59−4.53 (m, 1H), 4.42−4.38 (m, 1H), 4.35−4.31 (m, 1H), 1.94 (dd, J = 1.6, 1.0 Hz, 3H). ^{13}C NMR (101 MHz, chloroform-*d*): δ 167.19, 135.93, 126.25, 82.28, 80.59, 63.76, 63.56, 18.27. ^{19}F NMR (377 MHz, chloroform-*d*): δ −222.10.

Synthesis of P2FEMA_RAFT. P2FEMA_RAFT was prepared according to a previously reported literature procedure using Azobisisobutyronitrile (AIBN) as an initiator[27] The RAFT agent used in this work is 4-cyano-4-((phenylcarbonothioyl)thio)pentanoic acid.[30] The oven-dried Schlenk was charged with a stir bar and left to cool to room temperature under vacuum. The reagents were poured in sequence starting from 1 mL of dry DMF for each gram of monomer used, RAFT agent (1 equiv), AIBN (0.5 equiv), and the monomer 2FEMA [equiv = target(M_n)/monomer(M_w)] followed by four freeze−pump−thaw cycles to remove traces of oxygen. The Schlenk was then filled with argon, sealed, and left for 2 days at 50 °C under stirring. After cooling to room temperature, the solution or in the case of a solid dissolved in a minimum amount of THF (in some cases the solubilization required 2−4 h of sonication) was directly precipitated dropwise in pentane/methanol with an 8:2 ratio. The purification through precipitation was repeated twice to remove small traces of coupling defects. The M_n, dispersity ($Đ$), NMR, and yields of respective polymers are detailed in the Supporting Information (section 2.2).

Synthesis of SFEMA Diblock Copolymers. Following the guidelines of the previous synthesis, the oven-dried Schlenk was charged with a stir bar, 1 mL of dry DMF for each 0.3 g of P2FEMA_RAFT (1 equiv), AIBN (0.5 equiv), and the amount of styrene desired to have a range of M_n for different volume fractions. The vessel was subjected to three freeze−pump−thaw and then left stirring at 55 °C for 24 h. The mixture was directly precipitated dropwise in EtOH, 100 mL for each gram of polymer batch. In this case the precipitation was performed four times to guarantee an acceptable dispersity ($Đ$) of the polymer batches. The number-average molar masses (M_n), the weight-average molar masses (M_w), the molar mass distributions ($Đ = M_w/M_n$), and the volume fractions of SFEMA BCPs were determined by a combination of NMR and SEC. Volume fractions, M_n, $Đ$, NMR, and yields are detailed in the Supporting Information (section 2.3).

Nuclear Magnetic Resonance (NMR). NMR spectra were all recorded at ambient temperature by using a liquid-state 400 MHz NMR spectrometer (Bruker AVANCE I) with 5 mm BBFO probe in the appropriate deuterated solvent. Data are reported in chemical shift

Scheme 1. Process Flow for SFEMA Self-Assembly and AlO_x Nanowire Formation

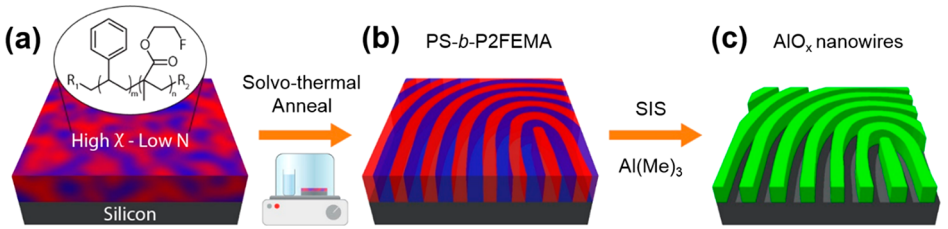

Scheme 2. Synthesis of SFEMA BCP Materials via Reversible Addition−Fragmentation Chain Transfer Polymerization

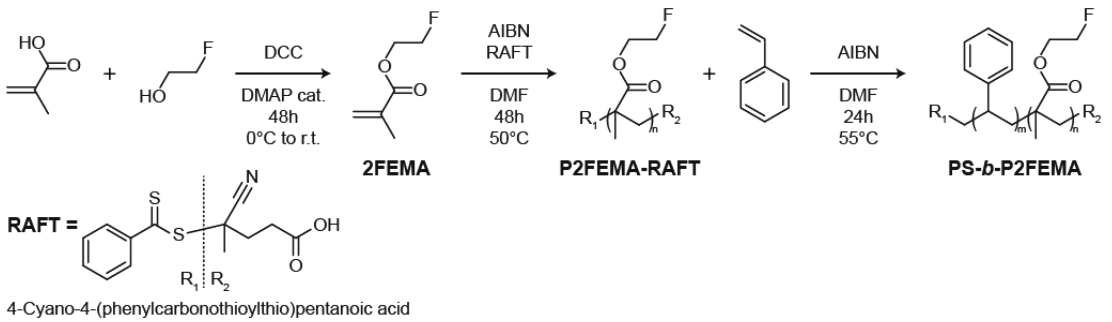

(ppm), multiplicity (s, singlet; d, doublet; t, triplet; dd, double doublet; q, quartet; the signals are referenced to the residual solvent DMSO-d_6 (δ = 2.50 ppm ^{1}H, 39.520 ppm 13C); $CDCl_3$ (δ = 7.26 ppm, 77.160 ppm ^{13}C); α,α,α-trifluorotoluene as internal standard (δ = −63.90 ppm).

Size Exclusion Chromatography (SEC). SEC measurements were performed with a Viscotek TDAmax system from Malvern Instruments that consists of an integrated solvent and sample delivery module (GPCmax) and a Tetra Detector Array (TDA). THF was used as the mobile phase at a flow rate of 0.8 mL/min and TCB as a flow rate marker. All polymers were injected (100 μL of solution) at a concentration of 5 mg/mL after filtration through a 0.45 μm pore-size membrane. The separation was performed on two Agilent columns [2 × PLgel 5 μm Mixed C (300 × 7.5 mm^2)] and a guard column (PL gel 5 μm). Columns and detectors were maintained at 30 °C. Relative molecular weights and dispersity were determined thanks to a conventional calibration obtained with polystyrene narrow standards.

Small-Angle X-ray Scattering (SAXS) Characterization. SAXS experiments were performed at the Centre de Recherche Paul Pascal (CRPP) at Université de Bordeaux using a high-resolution X-ray spectrometer Xeuss 2.0 from Xenoxs operating with radiation wavelength of λ = 1.54 Å. 2D scattering patterns were collected by using a PILATUS 300 K Dectris detector with a sample-to-detector distance of 1635 mm. The beam center position and the angular range were calibrated by using a silver behenate standard sample. The SAXS patterns were radially averaged around the direct beam position by using the Xenocs XSACT software. Temperature-dependent SAXS experiments were performed at the MINA (Multipurpose Instrument for Nanostructured Analysis) beamline in Groningen (Netherlands) by employing a rotating anode X-ray source with radiation wavelength of λ = 1.54 Å. The beam is collimated by using Monteil optics and a set of three Pt pinholes. The beam size at the sample position was 250 × 250 μm^2. SAXS patterns were recorded by using a Vantec2000 detector (Bruker) with pixel size 68 × 68 μm^2 placed 3000 mm away from the sample. The beam center and the sample-to-detector distance were calibrated by using the position of diffraction peaks from a standard silver behenate powder. The SAXS patterns were radially averaged around the direct beam position by using the Fit2D software. After radial averaging, the background signal from the empty cell was subtracted to all the sample profiles.

Thin Film Self-Assembly. Silicon substrates, with a native silicon dioxide layer (≈2 nm), were diced into 1 × 1 cm^2 pieces and ultrasonicated in toluene for 10 min. Prior to deposition, substrates were blown dry with N_2. Substrates were exposed to UV/O_3 for 10 min to remove any organic material and to hydroxylate the surface. Following treatment, 1−1.5 wt % SFEMA solutions were made up in toluene and left stirring until fully dissolved. SFEMA films were deposited upon the modified wafers at 4000 rpm for 30 s, with a ramp of 5 s. SFEMA films were subsequently exposed to chloroform or toluene solvent vapors in glass jars (total volume, 50 cm^3) from 1 to 30 min to induce self-assembly. For solvothermal vapor annealing, jars were placed on a hot plate at 50 °C.

Thin Film Characterization Methods. BCP surfaces were characterized by an atomic force microscope (AFM) using a Dimension FastScan AFM (Bruker) in tapping mode. Silicon cantilevers (Fastscan-A) with a typical tip radius of ≈5 nm were used. The resonance frequency of the cantilevers was ≈1.25 kHz. A JEOL 7800-E Prime scanning electron microscope (SEM) was used at low voltage acceleration (1 kV) in the superhigh-resolution gentle beam (GBSH) mode to characterize metal oxide nanostructures formed.

Atomic Layer Deposition (ALD) Exposure. Sequential infiltration synthesis (SIS) of AlO_x was performed by using an ALD (Ultratech SAVANNAH G2) tool in exposure mode. This mode allowed Al_2O_3 SIS using an alternating exposure of P2FEMA-based BCP thin films to trimethylaluminum (TMA) and deionized water at 80 °C with a purge under N_2 gas flow after each exposition.[31] During exposure time, pressure in the ALD chamber increased, leading to an infiltration of species in P2FEMA microdomains; then during purge time, unreacted precursor was removed by N_2 flow. Exposure and purge times used in this experiment were 60 and 300 s, respectively, for both precursors. Here we used three cycles (TMA/purge/H_2O/purge) of SIS to form AlO_x nanofeatures. Following SIS treatments, film were then plasma treated with O_2 plasma (60 W, 60 s, 20 sccm) to remove polymer and create AlO_x features.

RESULTS AND DISCUSSION

SFEMA Design, Synthesis, and Characterization. We have synthesized several lamellar and cylindrical forming PS-*b*-P2FEMA BCPs and examined their ability to form well-defined features for nanolithography. Our objectives included (i) patterning of sub-20 nm periods and feature sizes, (ii) demonstration of fast self-assembly, e.g., <5 min, and (iii) compatibility with standardized hardmask practices for potential pattern transfer. Scheme 1 outlines the overall

Table 1. Characteristics of SFEMA BCPs

BCP	M_n SEC[a] (kg mol^{-1})	M_n NMR[b] (kg mol^{-1})	$Đ$[a]	vol fract (P2FEMA/PS)[c]	d-spacing[d] (nm)	morphology (orientation)[d]	feature size[e] (nm)
SFEMA1	22	23.4	1.3	38/62	27.3	Lam (⊥)	10.2
SFEMA2	18	18.6	1.3	44/56	26.1	Lam (⊥)	10.1
SFEMA3	17	17.2	1.4	22/78	21.6	Hex (⊥)	9.4
SFEMA4	14	13.8	1.4	21/79	20.9	Hex (⊥)	11.9
SFEMA5	10	9.7	1.4	37/63	17.9	Lam (⊥)	8.3
SFEMA6	8	8.8	1.4	54/46	14.6	Lam (⊥)	8.1
SFEMA7	7	6.7	1.4	33/67	14.9	Lam (⊥)	7.3
SFEMA8	6.4	6.3	1.2	49/51		Dis	

[a]Molecular weights (M_n) and dispersity ($Đ$) evaluated by SEC using polystyrene standards. [b]Molecular weights (M_n) evaluated from ^{1}H NMR. [c]Volume fractions determined by ^{1}H NMR using the densities of PS (1.05 g/cm^3) and P2FEMA (1.27 g/cm^3 as measured by pycnometer) at 25 °C. [d]d-spacing obtained from SAXS with the morphologies determined by the q/q^* series, where q^* is the position of the first-order peak. Lam and Hex indicate lamellar and hexagonally packed cylindrical morphologies, respectively. [e]Respective feature sizes determined from AFM images.

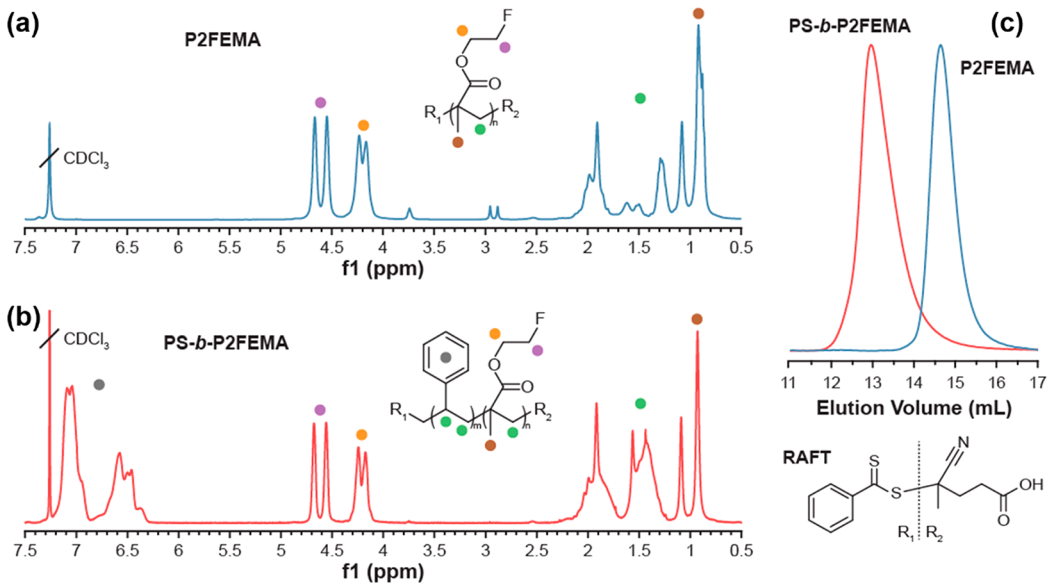

Figure 1. (a) ^{1}H NMR spectrum of P2FEMA-RAFT-A in chloroform-*d*. (b) ^{1}H NMR spectrum of SFEMA2 in chloroform-*d*. (c) SEC overlapped curves (P2FEMA-macro-RAFT is in blue and SFEMA2 is in red).

process flow for high χ–low N SFEMA BCPs, with the molecular structure shown in (a), SFEMA self-assembled patterns displayed in (b), and aluminum oxide (AlO_x) nanowires shown in (c) after sequential infiltration synthesis (SIS).

The synthesis and key characteristics of SFEMA BCPs synthesized by RAFT and studied in thin film form are outlined in Scheme 2 and Table 1. We have pursued the synthesis of a modified methyl methacrylate block functionalized with a single fluorine atom to develop a high χ BCP material. The reason for this pursuit is twofold. First, SFEMA BCPs of low molecular weight are capable of fabricating ultralow feature sizes (sub-10 nm), but critically the new materials do not exhibit large scale dewetting in thin film form as occurs in BCPs of vastly contrasting surface energies (e.g., PDMS containing BCPs).[32,33] Moreover, low-fluorinated polymerizable molecules are not commercially available, which provided further motivation for us to design and synthesize a monofluorinated derivative of ethyl methacrylate.

Using 2-fluoroethanol and methacrylic acid via a Steglich esterification with dicyclohexylcarbodiimide (DCC) as a condensating agent and (dimethylamino)pyridine (DMAP) as a catalyst, we routinely synthesized 2FEMA with high yield (over 80%). RAFT polymerization was chosen as it is a versatile technique allowing polymerization of a range of functionalized monomers (unlike anionic polymerization) and produces BCPs with low $Đ$ that are free of metal contamination. A standard, widely used RAFT agent was adopted to maintain a fast and approachable synthesis using commercially available reagents. 4-Cyano-4-(phenylcarbonothioylthio)pentanoic acid was used as the RAFT agent and azobis(isobutyronitrile) (AIBN) as a free radical initiator. The sequence of blocks was determined, as 2FEMA is much less reactive than styrene, and therefore the styrene-RAFT is not suitable. Thus, a series of P2FEMA-RAFT agents were synthesized and used to create desired SFEMA BCP materials. The polymers were characterized via nuclear magnetic resonance (NMR), SEC, and FT-IR, confirming the predicted structures (see the Supporting Information, section 2).

Figures 1a,b show the ^{1}H NMR spectra of the P2FEMA-macro-RAFT (top spectrum) and SFEMA2 (bottom spectrum). The ^{1}H NMR spectrum of SFEMA2 BCP clearly displays the aromatic group of the styrene from 6 to 7.5 ppm (grey dot), which is absent in the P2FEMA macro-RAFT (top). The aliphatic backbone is creating complex multiplets in between 1 and 2 ppm (green dots), while the methylenes of

the fluorinated ethanoate residue appear clearly as two doublets around 4.5 ppm in both P2FEMA-macro-RAFT and the SFEMA2 cases (purple and orange dots). Representative chromatograms are given in Figure 1c, showing the narrow dispersity for respective materials and the molecular mass increase, transitioning from the macro-RAFT (blue curve) to SFEMA2 (red curve).

Bulk Microphase Segregation. SFEMA BCP bulk phase behavior was probed by SAXS to establish respective BCP morphologies and domain spacing values. All samples were thermally annealed at 120 °C overnight prior to SAXS analysis. Measurements of the annealed samples were performed at 25 °C. Figure 2a displays SAXS patterns obtained for SFEMA1–7. The peaks observed confirmed the ability of these BCPs to form segregated structures in the bulk with M_n as low as 7 kg/mol. SFEMA BCPs labeled SFMEA1, SFMEA2, SFMEA5, SFEMA6, and SFEMA7 in Figure 2a display peaks positioned at q/q^* with ratios of 1:2:3:4 indicative of lamellar morphologies. Additionally, SAXS profiles of SFMEA3 and SFEMA4 show peak positions tentatively assigned to cylindrical systems in accordance with BCP composition and BCP thin film self-assembly behavior. Periods ranged from 27.3 to 14.6 nm for lamellar SFEMA BCPs ($d = 2\pi/q^*$, where d is the domain spacing and q^* is the primary peak position), as summarized in Table 1. Figure 2b displays the scaling relationship of lamellar BCP periods SFEMA1, -2, -5, and -6 versus the total degree of polymerization of respective BCPs based on 118 Å^3 reference volume. The experimental results for this series of SFEMA with a nearly constant composition exhibit a power law of $d \approx N^{0.62}$, in agreement with the strong segregation theory, i.e., $d \approx bN^{2/3}\chi^{1/6}$ where b is the statistical segment length.

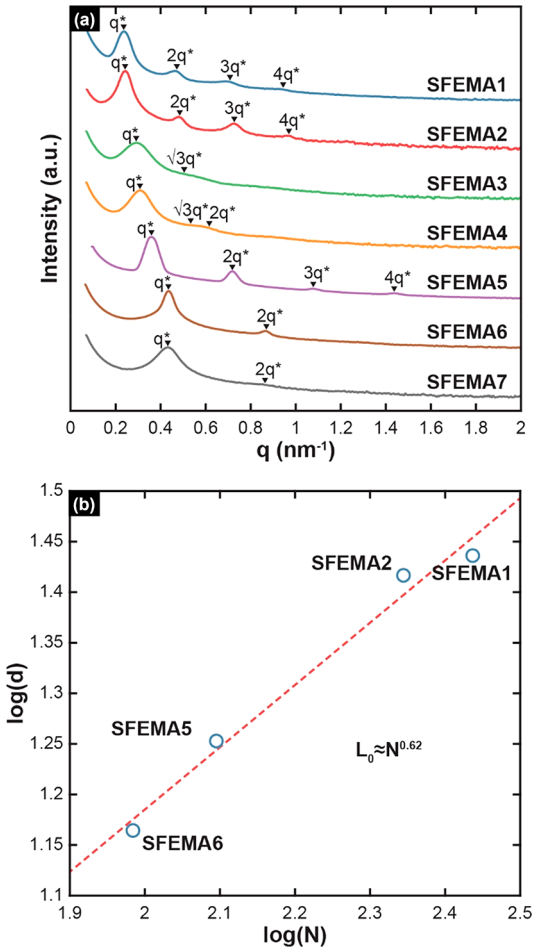

Figure 2. (a) Representative SAXS profiles acquired at 25 °C for bulk analysis of SFEMA BCPs. Data have been shifted vertically for clarity. (b) Plot of the scaling relationship of lamellar SFEMA BCP d-spacing (d) with respect to total degree of polymerization (N) based on 118 Å^3 reference volume for BCPs with a nearly constant composition.

Determination of χ for SFEMA. We subsequently determined the Flory–Huggins parameter of this system using temperature resolved SAXS. The absolute intensity calibrated with a low-density polyethylene standard was plotted against the primary scattering vector, q, for the disordered SFEMA8 sample (overall M_n = 6.4 kg/mol). A mean-field expression for the segment–segment interaction corrected from the effects of molecular weight dispersity and segmental volume asymmetry parameter has been extracted from these scattering profiles,[34−36] and the results are presented in Figure 3a (Supporting Information section 4 details the model used here together with data analysis carried

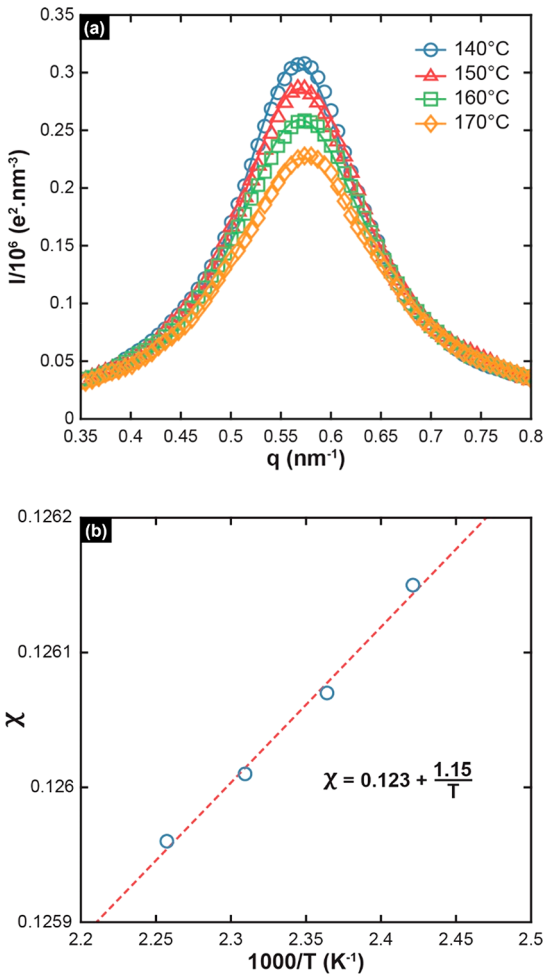

Figure 3. Determination of SFEMA χ by using Liebler mean-field theory. (a) Temperature-resolved SAXS intensity profiles of disordered SFEMA8 fitted by the mean-field theory at the vicinity of the scattering maximum associated with density fluctuations at 140 °C (blue circles), 150 °C (red triangles), 160 °C (green squares), and 170 °C (yellow diamonds). (b) Plot showing the linear dependence of χ calculated as a function of $1/T$.

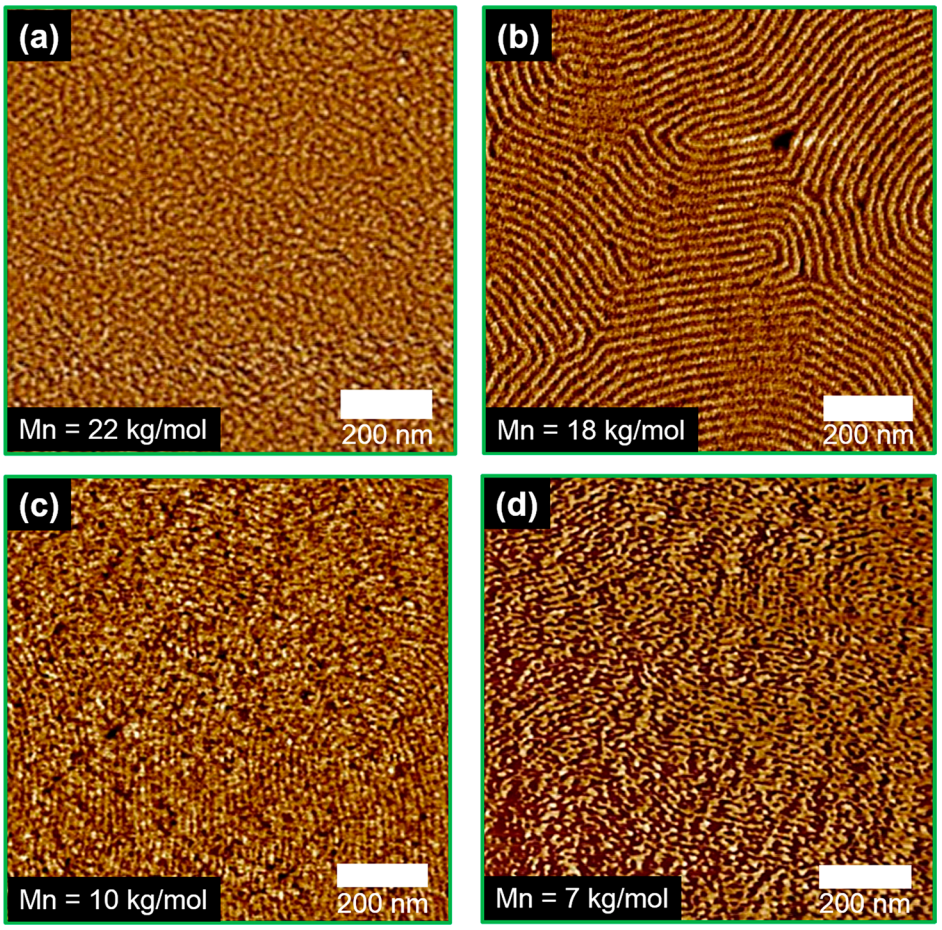

Figure 4. AFM phase images of self-assembled lamellar SFEMA BCP films on silicon surfaces with total molecular weights of (a) M_n = 22 kg/mol (SFEMA1), (b) M_n = 18 kg/mol (SFEMA2), (c) M_n = 10 kg/mol (SFEMA5), and (d) M_n = 7 kg/mol (SFEMA7). SFEMA films were solvothermal annealed in a $CHCl_3$ atmosphere at 50 °C for less than 3 min.

out). The resulting temperature-dependent Flory–Huggins parameter can be expressed as $\chi = 1.15 \times T^{-1} + 0.123$, which is equivalent to a value of 0.13 at 150 °C, over 4 times the value reported for PS-*b*-PMMA (0.03).[36] This value supersedes commercially available "high χ" BCPs including PS-*b*-PDMS (0.11) and PS-*b*-PLA (0.075).[37] Our SFEMA BCPs also challenge more recently published BCPs including poly(cyclohexylethylene)-*b*-PMMA (0.18)[38] and PMOST-*b*-PTMSS (0.046).[39] Such comparisons to the state-of-the-art literature illustrate the potential use of PS-*b*-P2FEMA for future nanomanufacturing.

SFEMA Thin Film Self-Assembly. Processing new BCPs in thin film form and precisely manipulating conditions to achieve desired orientation is paramount. Moreover, developing processes toward relevant features in rapid time scales is also desirable and is a central focus here. Lamellar BCP systems are extremely practical for pattern transfer as the vertical sidewalls of the original etch mask are advantageous for fidelity. Therefore, this section examines lamellar systems.

We screened several solvents to establish the optimum deposition conditions. PS is well-known to dissolve in toluene because of similar solubility values (Hansen solubility parameters for PS, δ_d = 18.6 $MPa^{1/2}$, δ_p = 1.0 $MPa^{1/2}$, δ_h = 4.1 $MPa^{1/2}$, and toluene, δ_d = 18.0 $MPa^{1/2}$, δ_p = 1.4 $MPa^{1/2}$, and δ_h = 2.0 $MPa^{1/2}$, where δ_d is the dispersive force, δ_p is the polar force, and δ_h is hydrogen bonding).[40] In addition, we also observed clear solutions from P2FEMA homopolymer–toluene solutions, inferring good solubility of P2FEMA in toluene. Thus, toluene was chosen for deposition of SFEMA and BCP film thicknesses were varied from ≈15 to 30 nm. Using such thin films is necessary to avoid image transfer issues during pattern transfer as pattern collapse of features is circumvented.[41]

We investigated SFEMA BCP self-assembly on UV/O_3-treated silicon and observed no large-scale dewetting of SFEMA BCPs. Initial experiments inferred the amenable nature of the PS and P2FEMA blocks materials on UV/O_3 modified silicon surfaces. However, as-cast films only exhibit ill-defined segregated structures (see Figure S29), and solvent vapor annealing was applied to the SFEMA films to increase polymer chain mobility and therefore enhance ordering of the resulting nanostructures. Additionally, such treatment allows to mitigate preferential interactions at the BCP bottom and top interfaces, thus promoting out-of-plane orientations of the BCP features. Cylinder systems were also investigated (and are detailed in Figure S30) to fabricate vertical nanofeatures and expand the overall applicability of the family of SFEMA BCPs synthesized. For lamellar systems, we observed microphase separation in thin films annealed under a chloroform or toluene atmosphere. Patterns were typically formed in less than 30 min. We subsequently examined the use of solvothermal annealing (STVA) at 50 °C to produce line-space features with larger correlation lengths. Moreover, STVA accelerates the

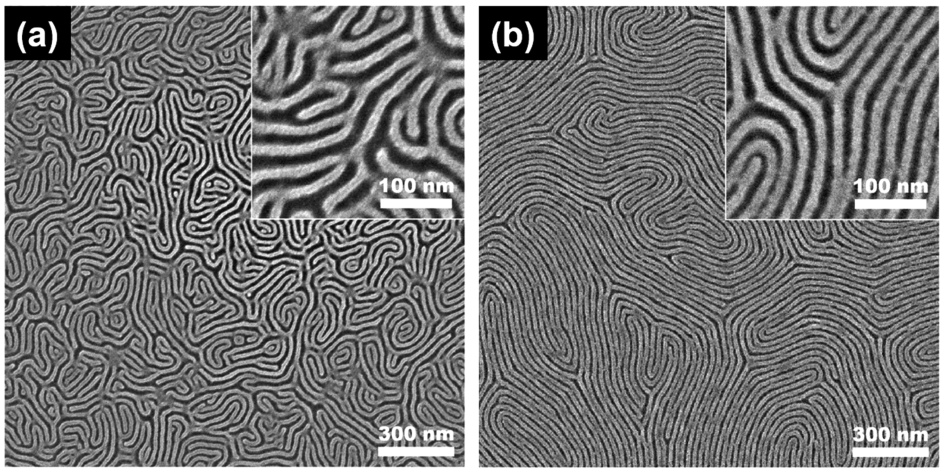

Figure 5. Large-area scanning electron microscopy image of AlO_x features developed from SIS treatment of (a) SFMEA 2 and (b) SFMEA5. Period is ≈25 nm with feature sizes ≈14 nm for SFMEA 2. Period is ≈18 nm with feature sizes ≈11 nm for SFEMA 5. Insets shows high-resolution images of AlO_x feature definition.

microphase separation[42−44] process to as short as 3 min (vide supra).

Figure 4a−d displays line-space features from SFEMA BCPs following STVA treatment for less than 3 min.The *d*-spacings were measured at 25.9 nm for SFMEA1 (Figure 4a), 24.5 nm for SFEMA2 (Figure 4b), 16.4 nm for SFEMA5 (Figure 4c), and 14.2 nm for SFEMA7 (Figure 4d). Despite other reports based on fluorine-containing BCPs requiring an etch procedure to reveal microdomains, we observed well-defined patterns after STVA alone. We assert that this is due to the presence of only one fluorine atom in the P2FEMA block. However, one should note that dewetting of films was observed after longer annealing periods, e.g., greater than 10 min, particularly in low molecular weight SFEMA (<10 kg mol^{-1}) which is possibly a result of the enhanced fluorine polymer block−solvent interaction at the free surface, resulting in film instability and ultimately leading to film rupture. However, longer annealing times were not required as microphase-separated patterns were observed in less than 3 min as evidenced in Figure 4.

Alumina Nanowire Fabrication. To be considered further for nanolithography applications, we evaluated the possibility of converting the P2FEMA block to a hardmask material. Hardmask formation is a desired attribute for semiconductor processing as it allows enhanced etching contrast for high aspect ratio features.[45−49] Enhanced etching can ultimately lead to better edge definition (lower line edge roughness) than all polymeric based BCPs. Given the chemical similarity between PMMA and P2FEMA which both share carbonyl groups, we used SIS to infiltrate the P2FEMA microdomains. After precursor exposure, films were subsequently oxygen plasma treated to create AlO_x nanowire replicas. The large-scale AlO_x line-space features shown in Figure 5 for SFEMA2 and SFEMA5 were exposed to three cycles of TMA/H_2O precursors. Highly defined features with excellent uniformity were observed (see the insets in Figure 5) demonstrating the versatility of SFEMA BCPs for nanolithography use.

A multitude of reasons make SFEMA BCPs synthesized here appealing for sub-10 nm nanolithography. First, the high χ (0.13 at 150 °C) nature allows access to small periods and interfacial widths at low *N*, which is a considerable barrier to further progression of PS-*b*-PMMA BCPs. Importantly, we have shown that fast self-assembly (in a matter of seconds) can be induced through STVA practices. It is also notable that SFEMA BCPs appear from our investigation not to present with a wetting layer at the polymer/air interface. This therefore eliminates the need for an additional trim plasma etch as required for silicon (and other)-containing BCPs. We suspect the absence of such a wetting layer is a result of P2FEMA possibly possessing a higher surface free energy value contrary to the more abundant fluorine-containing BCPs studied hitherto.

CONCLUSIONS

We have described the RAFT synthesis and characterization of a new fluorine-containing BCP system, PS-*b*-P2FEMA, for sub-10 nm nanolithography needs. The high χ (0.13 at 150 °C) SFEMA BCP modified with a fluorine-containing block favors rapid microphase separation even at low *N* (i.e., 7 kg/mol). Self-assembly of lamellar SFEMA was shown to form line-space patterns with periods of 14 nm in as short as 60 s. We have also evaluated the use of SFEMA thin films for generating well-defined AlO_x nanowires using industry compatible SIS. The rapid assembly and the compatibility demonstrated with SIS therefore position SFEMA BCPs as a useful candidate to pattern ultralow nanodimensions. In addition, we are currently exploring the thermal annealing of these materials given SFEMA block's relatively low T_g (≈ 90 °C), and results will be reported in due course to expand the processing options for this highly promising BCP material. Likewise, integrating such useful systems with directed self-assembly processes to dictate feature alignment will also be investigated.

ASSOCIATED CONTENT

Supporting Information

The Supporting Information is available free of charge at https://pubs.acs.org/doi/10.1021/acs.macromol.0c01148.

Experimental details; Figures S1−S30 (PDF)

AUTHOR INFORMATION

Corresponding Authors

Daniele Mantione − *CNRS, Bordeaux INP, LCPO, UMR 5629, Univ. Bordeaux, F-33600 Pessac, France;* orcid.org/

0000-0001-5495-9856; Email: daniele.mantione@u-bordeaux.fr

Guillaume Fleury − *CNRS, Bordeaux INP, LCPO, UMR 5629, Univ. Bordeaux, F-33600 Pessac, France;* orcid.org/0000-0003-0779-191X; Email: guillaume.fleury@u-bordeaux.fr

Authors

Cian Cummins − *CNRS, Bordeaux INP, LCPO, UMR 5629 and CNRS, Centre de Recherche Paul Pascal, UMR 5031, Univ. Bordeaux, F-33600 Pessac, France;* orcid.org/0000-0001-6338-3991

Federico Cruciani − *CNRS, Bordeaux INP, LCPO, UMR 5629, Univ. Bordeaux, F-33600 Pessac, France*

Guillaume Pino − *CNRS, Bordeaux INP, LCPO, UMR 5629, Univ. Bordeaux, F-33600 Pessac, France*

Nils Demazy − *CNRS, Bordeaux INP, LCPO, UMR 5629, Univ. Bordeaux, F-33600 Pessac, France*

Yulin Shi − *Zernike Institute for Advanced Materials, University of Groningen, NL-9747 AG Groningen, The Netherlands*

Giuseppe Portale − *Zernike Institute for Advanced Materials, University of Groningen, NL-9747 AG Groningen, The Netherlands;* orcid.org/0000-0002-4903-3159

Georges Hadziioannou − *CNRS, Bordeaux INP, LCPO, UMR 5629, Univ. Bordeaux, F-33600 Pessac, France;* orcid.org/0000-0002-7377-6040

■ ACKNOWLEDGMENTS

The authors are sincerely grateful for financial support from the University of Bordeaux and the LabEx AMADEus (ANR-10-LABEX-0042-AMADEUS). The authors thank Ahmed Bentaleb (CRPP, University of Bordeaux) for SAXS assistance. The authors also thank the LCPO support staff—Aude Manson, Melanie Bousquet, Ellena Karnezis, and Gilles Pecastaings—for their endless everyday help. This work was performed within the framework of the Equipex ELORPrint-Tec ANR-10-EQPX-28-01 with the help of the French state's Initiative d'Excellence IdEx ANR-10-IDEX-003-02.

■ REFERENCES

(1) Orilall, M. C.; Wiesner, U. Block copolymer based composition and morphology control in nanostructured hybrid materials for energy conversion and storage: solar cells, batteries, and fuel cells. *Chem. Soc. Rev.* **2011**, *40* (2), 520−535.

(2) Abetz, V. Isoporous Block Copolymer Membranes. *Macromol. Rapid Commun.* **2015**, *36* (1), 10−22.

(3) Hu, H.; Gopinadhan, M.; Osuji, C. O. Directed self-assembly of block copolymers: a tutorial review of strategies for enabling nanotechnology with soft matter. *Soft Matter* **2014**, *10* (22), 3867−3889.

(4) Demazy, N.; Cummins, C.; Aissou, K.; Fleury, G. Non-Native Block Copolymer Thin Film Nanostructures Derived from Iterative Self-Assembly Processes. *Adv. Mater. Interfaces* **2020**, *7* (5), 1901747.

(5) Gabinet, U. R.; Osuji, C. O. Optical materials and metamaterials from nanostructured soft matter. *Nano Res.* **2019**, *12* (9), 2172−2183.

(6) Luo, Y.; Montarnal, D.; Kim, S.; Shi, W.; Barteau, K. P.; Pester, C. W.; Hustad, P. D.; Christianson, M. D.; Fredrickson, G. H.; Kramer, E. J.; Hawker, C. J. Poly(dimethylsiloxane-b-methyl methacrylate): A Promising Candidate for Sub-10 nm Patterning. *Macromolecules* **2015**, *48* (11), 3422−3430.

(7) Pitet, L. M.; Wuister, S. F.; Peeters, E.; Kramer, E. J.; Hawker, C. J.; Meijer, E. W. Well-Organized Dense Arrays of Nanodomains in Thin Films of Poly(dimethylsiloxane)-*b*-poly(lactide) Diblock Copolymers. *Macromolecules* **2013**, *46* (20), 8289−8295.

(8) Ji, S.; Wan, L.; Liu, C.-C.; Nealey, P. F. Directed self-assembly of block copolymers on chemical patterns: A platform for nanofabrication. *Prog. Polym. Sci.* **2016**, *54*, 76−127.

(9) Cummins, C.; Morris, M. A. Using block copolymers as infiltration sites for development of future nanoelectronic devices: Achievements, barriers, and opportunities. *Microelectron. Eng.* **2018**, *195*, 74−85.

(10) Bates, C. M.; Maher, M. J.; Janes, D. W.; Ellison, C. J.; Willson, C. G. Block Copolymer Lithography. *Macromolecules* **2014**, *47* (1), 2−12.

(11) Maher, M. J.; Mori, K.; Sirard, S. M.; Dinhobl, A. M.; Bates, C. M.; Gurer, E.; Blachut, G.; Lane, A. P.; Durand, W. J.; Carlson, M. C.; Strahan, J. R.; Ellison, C. J.; Willson, C. G. Pattern Transfer of Sub-10 nm Features via Tin-Containing Block Copolymers. *ACS Macro Lett.* **2016**, *5* (3), 391−395.

(12) Bates, F. S.; Fredrickson, G. H. Block Copolymer Thermodynamics - Theory and Experiment. *Annu. Rev. Phys. Chem.* **1990**, *41*, 525−557.

(13) Cummins, C.; Ghoshal, T.; Holmes, J. D.; Morris, M. A. Strategies for Inorganic Incorporation using Neat Block Copolymer Thin Films for Etch Mask Function and Nanotechnological Application. *Adv. Mater. (Weinheim, Ger.)* **2016**, *28* (27), 5586−618.

(14) Bates, C. M.; Seshimo, T.; Maher, M. J.; Durand, W. J.; Cushen, J. D.; Dean, L. M.; Blachut, G.; Ellison, C. J.; Willson, C. G. Polarity-Switching Top Coats Enable Orientation of Sub-10-nm Block Copolymer Domains. *Science* **2012**, *338* (6108), 775−779.

(15) Lane, A. P.; Yang, X.; Maher, M. J.; Blachut, G.; Asano, Y.; Someya, Y.; Mallavarapu, A.; Sirard, S. M.; Ellison, C. J.; Willson, C. G. Directed Self-Assembly and Pattern Transfer of Five Nanometer Block Copolymer Lamellae. *ACS Nano* **2017**, *11* (8), 7656−7665.

(16) Cushen, J.; Wan, L.; Blachut, G.; Maher, M. J.; Albrecht, T. R.; Ellison, C. J.; Willson, C. G.; Ruiz, R. Double-Patterned Sidewall Directed Self-Assembly and Pattern Transfer of Sub-10 nm PTMSS-b-PMOST. *ACS Appl. Mater. Interfaces* **2015**, *7* (24), 13476−13483.

(17) Aissou, K.; Mumtaz, M.; Fleury, G.; Portale, G.; Navarro, C.; Cloutet, E.; Brochon, C.; Ross, C. A.; Hadziioannou, G. Sub-10 nm Features Obtained from Directed Self-Assembly of Semicrystalline Polycarbosilane-Based Block Copolymer Thin Films. *Adv. Mater.* **2015**, *27* (2), 261−265.

(18) Li, M.; Douki, K.; Goto, K.; Li, X.; Coenjarts, C.; Smilgies, D. M.; Ober, C. K. Spatially Controlled Fabrication of Nanoporous Block Copolymers. *Chem. Mater.* **2004**, *16* (20), 3800−3808.

(19) Bosworth, J. K.; Paik, M. Y.; Ruiz, R.; Schwartz, E. L.; Huang, J. Q.; Ko, A. W.; Smilgies, D.-M.; Black, C. T.; Ober, C. K. Control of Self-Assembly of Lithographically Patternable Block Copolymer Films. *ACS Nano* **2008**, *2* (7), 1396−1402.

(20) Bosworth, J. K.; Black, C. T.; Ober, C. K. Selective Area Control of Self-Assembled Pattern Architecture Using a Lithographically Patternable Block Copolymer. *ACS Nano* **2009**, *3* (7), 1761−1766.

(21) Wang, C.; Li, X.; Deng, H. Synthesis of a Fluoromethacrylate Hydroxystyrene Block Copolymer Capable of Rapidly Forming Sub-5 nm Domains at Low Temperatures. *ACS Macro Lett.* **2019**, *8* (4), 368−373.

(22) Azuma, K.; Sun, J.; Choo, Y.; Rokhlenko, Y.; Dwyer, J. H.; Schweitzer, B.; Hayakawa, T.; Osuji, C. O.; Gopalan, P. Self-Assembly of an Ultrahigh-χ Block Copolymer with Versatile Etch Selectivity. *Macromolecules* **2018**, *51* (16), 6460−6467.

(23) Kwak, J.; Mishra, A. K.; Lee, J.; Lee, K. S.; Choi, C.; Maiti, S.; Kim, M.; Kim, J. K. Fabrication of Sub-3 nm Feature Size Based on Block Copolymer Self-Assembly for Next-Generation Nanolithography. *Macromolecules* **2017**, *50* (17), 6813−6818.

(24) Kanimozhi, C.; Kim, M.; Larson, S. R.; Choi, J. W.; Choo, Y.; Sweat, D. P.; Osuji, C. O.; Gopalan, P. Isomeric Effect Enabled Thermally Driven Self-Assembly of Hydroxystyrene-Based Block Copolymers. *ACS Macro Lett.* **2016**, *5* (7), 833−838.
(25) Maeda, R.; Hayakawa, T.; Ober, C. K. Dual Mode Patterning of Fluorine-Containing Block Copolymers through Combined Top-down and Bottom-up Lithography. *Chem. Mater.* **2012**, *24* (8), 1454−1461.
(26) Brassat, K.; Lindner, J. K. N. Nanoscale Block Copolymer Self-Assembly and Microscale Polymer Film Dewetting: Progress in Understanding the Role of Interfacial Energies in the Formation of Hierarchical Nanostructures. *Adv. Mater. Interfaces* **2020**, *7* (5), 1901565.
(27) Nakatani, R.; Takano, H.; Chandra, A.; Yoshimura, Y.; Wang, L.; Suzuki, Y.; Tanaka, Y.; Maeda, R.; Kihara, N.; Minegishi, S.; Miyagi, K.; Kasahara, Y.; Sato, H.; Seino, Y.; Azuma, T.; Yokoyama, H.; Ober, C. K.; Hayakawa, T. Perpendicular Orientation Control without Interfacial Treatment of RAFT-Synthesized High-χ Block Copolymer Thin Films with Sub-10 nm Features Prepared via Thermal Annealing. *ACS Appl. Mater. Interfaces* **2017**, *9* (37), 31266−31278.
(28) Jo, S.; Jeon, S.; Jun, T.; Park, C.; Ryu, D. Y. Fluorine-Containing Styrenic Block Copolymers toward High χ and Perpendicular Lamellae in Thin Films. *Macromolecules* **2018**, *51* (18), 7152−7159.
(29) Li, X.; Li, J.; Wang, C.; Liu, Y.; Deng, H. Fast self-assembly of polystyrene-b-poly(fluoro methacrylate) into sub-5 nm microdomains for nanopatterning applications. *J. Mater. Chem. C* **2019**, *7* (9), 2535−2540.
(30) Moad, G.; Rizzardo, E.; Thang, S. H. Living Radical Polymerization by the RAFT Process − A Third Update. *Aust. J. Chem.* **2012**, *65* (8), 985−1076.
(31) Peng, Q.; Tseng, Y.-C.; Darling, S. B.; Elam, J. W. A Route to Nanoscopic Materials via Sequential Infiltration Synthesis on Block Copolymer Templates. *ACS Nano* **2011**, *5* (6), 4600−4606.
(32) Girardot, C.; Böhme, S.; Archambault, S.; Salaün, M.; Latu-Romain, E.; Cunge, G.; Joubert, O.; Zelsmann, M. Pulsed Transfer Etching of PS−PDMS Block Copolymers Self-Assembled in 193 nm Lithography Stacks. *ACS Appl. Mater. Interfaces* **2014**, *6* (18), 16276−16282.
(33) Borah, D.; Cummins, C.; Rasappa, S.; Senthamaraikannan, R.; Salaun, M.; Zelsmann, M.; Liontos, G.; Ntetsikas, K.; Avgeropoulos, A.; Morris, A. M. Nanopatterning via Self-Assembly of a Lamellar-Forming Polystyrene-*block*-Poly(dimethylsiloxane) Diblock Copolymer on Topographical Substrates Fabricated by Nanoimprint Lithography. *Nanomaterials* **2018**, *8* (1), 32.
(34) Leibler, L. Theory of Microphase Separation in Block Copolymers. *Macromolecules* **1980**, *13* (6), 1602−1617.
(35) Sakurai, S.; Mori, K.; Okawara, A.; Kimishima, K.; Hashimoto, T. Evaluation of segmental interaction by small-angle x-ray scattering based on the random-phase approximation for asymmetric, polydisperse triblock copolymers. *Macromolecules* **1992**, *25* (10), 2679−2691.
(36) Zhao, Y.; Sivaniah, E.; Hashimoto, T. SAXS Analysis of the Order−Disorder Transition and the Interaction Parameter of Polystyrene-*block*-poly(methyl methacrylate). *Macromolecules* **2008**, *41* (24), 9948−9951.
(37) Sinturel, C.; Bates, F. S.; Hillmyer, M. A. High χ−Low N Block Polymers: How Far Can We Go? *ACS Macro Lett.* **2015**, *4* (9), 1044−1050.
(38) Kennemur, J. G.; Yao, L.; Bates, F. S.; Hillmyer, M. A. Sub-5 nm Domains in Ordered Poly(cyclohexylethylene)-*block*-poly(methyl methacrylate) Block Polymers for Lithography. *Macromolecules* **2014**, *47* (4), 1411−1418.
(39) Durand, W. J.; Blachut, G.; Maher, M. J.; Sirard, S.; Tein, S.; Carlson, M. C.; Asano, Y.; Zhou, S. X.; Lane, A. P.; Bates, C. M.; Ellison, C. J.; Willson, C. G. Design of high-χ block copolymers for lithography. *J. Polym. Sci., Part A: Polym. Chem.* **2015**, *53* (2), 344−352.
(40) Hansen, C. M. *Hansen Solubility Parameters: A User's Handbook*; CRC Press: 2007.
(41) Ruiz, R.; Wan, L.; Lille, J.; Patel, K. C.; Dobisz, E.; Johnston, D. E.; Kisslinger, K.; Black, C. T. Image quality and pattern transfer in directed self assembly with block-selective atomic layer deposition. *J. Vac. Sci. Technol., B: Nanotechnol. Microelectron.: Mater., Process., Meas., Phenom.* **2012**, *30* (6), 06F202.
(42) Cummins, C.; Mokarian-Tabari, P.; Andreazza, P.; Sinturel, C.; Morris, M. A. Solvothermal Vapor Annealing of Lamellar Poly(styrene)-*block*-poly(d,l-lactide) Block Copolymer Thin Films for Directed Self-Assembly Application. *ACS Appl. Mater. Interfaces* **2016**, *8* (12), 8295−8304.
(43) Gotrik, K. W.; Ross, C. A. Solvothermal Annealing of Block Copolymer Thin Films. *Nano Lett.* **2013**, *13* (11), 5117−5122.
(44) Lundy, R.; Flynn, S. P.; Cummins, C.; Kelleher, S. M.; Collins, M. N.; Dalton, E.; Daniels, S.; Morris, M. A.; Enright, R. Controlled solvent vapor annealing of a high [small chi] block copolymer thin film. *Phys. Chem. Chem. Phys.* **2017**, *19* (4), 2805−2815.
(45) Cummins, C.; Gangnaik, A.; Kelly, R. A.; Borah, D.; O'Connell, J.; Petkov, N.; Georgiev, Y. M.; Holmes, J. D.; Morris, M. A. Aligned silicon nanofins via the directed self-assembly of PS-b-P4VP block copolymer and metal oxide enhanced pattern transfer. *Nanoscale* **2015**, *7* (15), 6712−6721.
(46) Cummins, C.; Gangnaik, A.; Kelly, R. A.; Hydes, A. J.; O'Connell, J.; Petkov, N.; Georgiev, Y. M.; Borah, D.; Holmes, J. D.; Morris, M. A. Parallel Arrays of Sub-10 nm Aligned Germanium Nanofins from an In Situ Metal Oxide Hardmask using Directed Self-Assembly of Block Copolymers. *Chem. Mater.* **2015**, *27* (17), 6091−6096.
(47) Tseng, Y.-C.; Peng, Q.; Ocola, L. E.; Czaplewski, D. A.; Elam, J. W.; Darling, S. B. Etch properties of resists modified by sequential infiltration synthesis. *J. Vac. Sci. Technol., B: Nanotechnol. Microelectron.: Mater., Process., Meas., Phenom.* **2011**, *29* (6), 06FG01.
(48) Tseng, Y.-C.; Peng, Q.; Ocola, L. E.; Elam, J. W.; Darling, S. B. Enhanced Block Copolymer Lithography Using Sequential Infiltration Synthesis. *J. Phys. Chem. C* **2011**, *115* (36), 17725−17729.
(49) Tseng, Y.-C.; Mane, A. U.; Elam, J. W.; Darling, S. B. Enhanced Lithographic Imaging Layer Meets Semiconductor Manufacturing Specification a Decade Early. *Adv. Mater.* **2012**, *24* (19), 2608−2613.